Magnetic-field-induced gapless state in multiband superconductors

Victor Barzykin
National High Magnetic Field Laboratory, Florida State University, Tallahassee, Florida 32310, USA
(Received 9 July 2008; published 21 April 2009)

We investigate theoretically the properties of *s*-wave multiband superconductors in the weak-coupling (BCS) limit in the presence of pair-breaking effects of magnetic field. It is shown that a gapless superconducting state must appear in quasi-two-dimensional superconductors in magnetic fields parallel to the plane, corresponding to a Sarma state induced on one of the Fermi surfaces. The emergence of the state in *s*-wave multiband superconductors in the absence of anisotropy or spin-orbit interaction is usually accompanied by a zero-temperature first-order metamagnetic phase transition. For anisotropic or non-*s*-wave multiband superconductors the order of the zero-temperature metamagnetic transition depends on model parameters, and it may take the form of a smooth crossover. The details of the temperature–magnetic-field phase diagram for multiband superconductors are investigated analytically at zero temperature and numerically at a finite temperature. It is shown the zero-temperatures first-order phase transition gives rise to a critical region on the *B*-*T* phase diagram. We suggest possible experiments to detect the gapless state.

DOI: 10.1103/PhysRevB.79.134517 PACS number(s): 74.20.−z, 74.25.Ha, 74.70.Tx, 74.70.Kn

I. INTRODUCTION

Superconductivity in multiband metals was first investigated theoretically shortly after the BCS theory.[1–5] A resurgence of interest in multiband superconductivity has been mostly related to experimental discovery of MgB_2,[6] and observation of the two *s*-wave gaps by various techniques.[7–14] Recent discovery of iron oxypnictides,[15] a new family of quasi-two-dimensional (2D) high-temperature superconductors, has also attracted enormous theoretical interest to the problem of multiband superconductivity. First-principles numerical band-structure calculations[16–18] show that several bands cross the Fermi level in these materials. While the pairing mechanism in iron oxypnictides is not yet clear, several bands are involved in the determination of both normal and superconducting properties.[18,19] The existence of multiband energy spectrum[20] and associated several energy gaps[21,22] was also verified experimentally in an older, quasi-2D *s*-wave superconductor $NbSe_2$. BCS investigations of multiband superconductivity were restarted,[23,24] but were mostly centered around the physics that arises due to the presence of two separate gaps. The multiband energy spectrum is also present in most unconventional heavy fermion superconductors due to extreme complexity of the band structure of these materials, as indicated by de Haas–van Alfven measurements. For example, gapless superconductivity of Abrikosov-Gor'kov type[25] was recently observed in thermal-conductivity data for La-doped $CeCoIn_5$,[26] as indicated by unusual Wiedeman-Franz $1/x$ behavior of thermal conductivity at small concentration of La, x. The unusual behavior was attributed to the multiband structure[26,27] of this material, a *d*-wave superconductor.

Theoretical study of multiband superconductivity has not only been motivated by the above compounds. A somewhat modified multiband model is applicable to other new materials,[28] where a single Fermi surface gets spin split into two pieces with different Fermi momenta due to interactions, such as superconductors without center of inversion (CI) (Ref. 29) [for example, $CePt_3Si$ (Ref. 30)], or ferromagnetic superconductors [UGe_2,[31,32] $ZrZn_2$,[33] or URhGe (Ref. 34)]. A particular case of CI-symmetry breaking is two-dimensional surface superconductivity,[35,36] where two Fermi surfaces arise as a result of spin-orbit interaction of Rashba form.[37,38]

The Fermi surface will also get spin split in exchange field, an external magnetic field without orbital effects. Theoretically, paramagnetic pair breaking by exchange field corresponds to the old problem of unbalanced pairing, first studied in the early 60's,[39–44] when the *B*-*T* phase diagram for three-dimensional materials in exchange field has first been obtained. Orbital effects are almost always present in three dimensions, and even in very anisotropic quasi-2D materials, unless H_{c2} in magnetic fields parallel to the 2D plane close to Clogston paramagnetic limit.[39,40] This is, perhaps, the reason why the consequences of the theory have not studied in detail experimentally. A study of thin films in magnetic fields parallel to the surface remains, perhaps, the most promising experimental setup for the observation of unbalanced pairing in superconductors.[45–47] A possible observation of the Larkin-Ovchinnikov-Fulde-Ferrel (LOFF) (Refs. 41 and 42) has also been reported in some quasi-2D superconductors, such as those based on charge-transfer organic salts of BEDT-TTF or ET–ion[48] and the 1–1-5 family heavy fermion materials.[49–53]

While most theoretical studies of superconductivity in multiband compounds concentrated on the mechanism of superconductivity and the effects of several energy gaps on superconducting properties, some recent studies[54] found that a new class of superfluids could potentially arise in these materials, one that features coexistence of fully gapped and gapless states. For the most part, this class of states was proposed in Bose-Einstein condensation for different nonidentical fermions condensed by an optical trap,[55] or in high-energy physics,[56] where the "breached" superfluid state appears as a result of pairing between different quarks[57,58] in the asymptotically free limit.

Gapless solutions of this type were previously known, but in most cases were found to be energetically unstable. The first example corresponds to the second unstable solution in the unbalanced pairing problem, and is commonly referred to

as Sarma state.[43,44] The second solution of the gap equation for a superconductor placed in an exchange field was first obtained by the Green's functions method by Baltensperger[59] and Gor'kov and Rusinov,[60] where it was found to be energetically unstable. The exact nature of this unstable state and the existence of unpaired electron- and hole-Fermi surfaces were later clarified within BCS theory by Sarma and Takada.[43,44] The second example is pairing in a doped (unbalanced) excitonic gas, leading to an excitonic condensate,[61,62] which is actually the same two-band unbalanced pairing problem as one considered by Liu and Wilczek.[55] The solution previously found for this problem takes the form of a magnetically (ferromagnetically or antiferromagnetically) polarized gapless state,[63,64] and is different from "interior gap superfluid" of Liu and Wilczek. Similar to Sarma state, this solution is usually unstable with respect to formation of LOFF state or domains,[65–67] although the stability of this magnetic solution has not been fully investigated as a function of masses involved. The third example is the Sarma gapless state, which appears in the problem of *s*-wave pairing in ferromagnetic superconductors.[68] While it has been claimed[68] that Sarma state is stabilized by the presence of ferromagnetic order, this claim has been debated later.[69,70] According to recent work of Liu and Wilczek, a large difference in effective masses on two Fermi surfaces tends to stabilize the "breached" superfluid state already within the unbalanced pairing problem.[55]

The main motivation for this paper is a detailed theoretical study of possible gapless states in multiband superconductors in the presence of exchange magnetic field,[71] or the multiband unbalanced pairing problem. While certain similarity does exist, the multiband problem is really different[72] from the unbalanced pairing problem considered in the above cases; pairing between two different species of fermions (two different bands) is usually not a relevant mechanism in multiband superconductors since the energy difference for the two bands, $\Delta\epsilon \sim 1$ eV is much greater than $T_c \sim 1$ K. Nevertheless, for a superconductor placed in an external "exchange" field the unbalanced pairing problem is recovered. Surprisingly, as it was shown in Ref. 71, the multiband structure often leads to a stabilization of unusual Sarma state on the second band in exchange fields $\mu_B B > \Delta_2$, where Δ_2 is the energy band on the second Fermi surface. Thus, in quasi-2D superconductors where several bands cross the Fermi surface, such as $CeCoIn_5$ or 2H-$NbSe_2$, the peculiarities of the B-T phase diagram may not limited to high magnetic fields, where the LOFF-related phenomena are observed. New singularities and gapless states associated with the gaps on secondary Fermi surfaces must arise in *low* magnetic fields as well.[71] They correspond to the appearance of Sarma state[43] on the Fermi surface with smaller gap, one that becomes energetically stable due to the presence of the superconducting gap on the other Fermi surface. This state is characterized[43] by the presence of unpaired spin-polarized electrons near the Fermi surface of the second band, two open electron- and hole-Fermi surfaces, a paramagnetic magnetic moment and a first-order phase transition that always accompanies the appearance of this unusual state in *s*-wave multiband superconductors in low magnetic fields.[71]

The paper is organized as follows. In Sec. II we introduce the multiband model and generalize its known solution in the *s*-wave case to include effects of gap anisotropy and non-*s*-wave pairing symmetry. We demonstrate that the effective coupling constants can be eliminated in favor of the measurable parameters for multiband superconductors, such as the superconducting transition temperature, T_c, and the ratio of the gap amplitudes and the densities of states on different Fermi surfaces. In particular, thermodynamics of multiband superconductors is additive; the thermodynamic potential Ω is a simple BCS sum over different bands. In Sec. III we consider the problem of paramagnetic pair breaking in multiband superconductors and show that a gapless state is energetically stable in low magnetic fields in some region of model parameters. We investigate the stability and the magnetic properties of this gapless state in an *s*-wave two-band superconductor analytically at $T=0$, and provide the details for the B-T phase diagram and the low-temperature critical point that separates the partially gapless state from fully gapped state. In Sec. IV we present our conclusions.

II. MULTIBAND MODEL IN THE WEAK-COUPLING LIMIT

In a standard BCS approach[73] the pairing interaction can always be eliminated in favor of a single energy scale, T_c, giving rise to the well-known universality of the BCS theory. The critical temperature T_c is the only parameter that determines thermodynamic, kinetic, and other properties in the weak-coupling limit. For example, the superconducting gap at zero temperature, $\Delta(0)$, is related to T_c in *s*-wave superconductors by the universal law, $\Delta(0)=(\pi/\gamma)T_c \simeq 1.76T_c$. Similar universality is applicable to non-*s*-wave superconductors as well, even though the universal ratio $\Delta(0)/T_c$ depends on the type of pairing. For *d*-wave pairing, the weak-coupling ratio of the maximum gap amplitude at $T=0$ to T_c is $\Delta(0)/T_c=2\pi T_c/\gamma\sqrt{e} \simeq 2.14$.[74] Since a number of interaction parameters are involved in a multiband model, there is no such universal relation between $\Delta_\alpha(0)$ on different Fermi surfaces and T_c. Thus, T_c cannot be the only parameter that describes the properties of multiband superconductors. Geilikman, Zaitsev, and Kresin[3,4] showed using the method of Pokrovskii[75] that some universality is left in the weak-coupling multiband model. First, the physical properties, such as thermodynamics, are often additive over different bands. Second, the ratios of the gap amplitudes on different Fermi surfaces are temperature independent in the weak-coupling limit. Third, Geilikman *et al.*[3] found that all physical properties of a BCS multiband superconductor can be expressed in terms of the transition temperature T_c, and other quantities measurable in the normal state, such as the ratios of densities of states on different Fermi surfaces, and the temperature-independent ratio gap amplitudes. The gap amplitudes themselves, however, are not universal. In this section we introduce the multiband model, review some of the results of Geilikman *et al.*[3] that we will use in other sections, and generalize their weak-coupling solution to the case of arbitrary anisotropic pairing.

The Hamiltonian for several separate Fermi surfaces has the following form (see, for example, Ref. 72):

$$H_{el} = \sum_{\alpha\sigma\boldsymbol{k}} \epsilon(\boldsymbol{k}) a^{\dagger}_{\alpha\sigma}(\boldsymbol{k}) a_{\alpha\sigma}(\boldsymbol{k}) + \frac{1}{2}\sum_{\boldsymbol{k},\boldsymbol{k}'} \sum_{\alpha\beta\sigma_{1-4}} V_{\alpha\beta\sigma_{1-4}}(\boldsymbol{k},\boldsymbol{k}') \times a^{\dagger}_{\alpha\sigma_1}(-\boldsymbol{k}) a^{\dagger}_{\alpha\sigma_2}(\boldsymbol{k}) a_{\beta\sigma_3}(\boldsymbol{k}') a_{\beta\sigma_4}(-\boldsymbol{k}'), \quad (1)$$

where σ_{1-4} are spin indices and $V_{\alpha\beta\sigma_{1-4}}(\boldsymbol{k},\boldsymbol{k}')$ corresponds to the model interaction for a pair of electrons from band β with quasimomentum $\boldsymbol{k}'$ to band α with quasimomentum $\boldsymbol{k}$. The latter can be written in the following form:

$$V_{\alpha\beta\sigma_{1-4}}(\boldsymbol{k},\boldsymbol{k}') = V_{\alpha\beta}(\boldsymbol{k},\boldsymbol{k}')(i\sigma_y)_{\sigma_1\sigma_2}(i\sigma_y)^{\dagger}_{\sigma_3\sigma_4}. \quad (2)$$

Note that the unbalanced pairing terms[55,57,58] are not present in this model BCS formulation since the mismatch between different Fermi surfaces is usually too large (of the order of ~eV) for these terms to be relevant. We consider below any possible type of the superconducting state. As usual, the interactions in the model BCS Hamiltonian are taken in a factorized form,

$$V_{\alpha\beta}(\boldsymbol{k};\boldsymbol{k}') = \chi(\varphi,\theta) V_{\alpha\beta} \chi(\varphi',\theta'), \quad (3)$$

where $\chi(\varphi,\theta)$ is the appropriate irreducible representation, normalized to unity

$$\int \frac{d\Omega}{4\pi} |\chi(\varphi,\theta)|^2 = 1. \quad (4)$$

For example, for the s-wave pairing

$$\chi(\varphi,\theta) = 1, \quad (5)$$

while for the d-wave pairing,

$$\chi(\varphi,\theta) = \sqrt{2}\cos(2\varphi). \quad (6)$$

The energy gaps on each Fermi surface $\Delta_\alpha(\boldsymbol{k})$ can be easily expressed in terms of the interaction matrix $V_{\alpha\beta}(\boldsymbol{k};\boldsymbol{k}')$ and the anomalous Gor'kov functions $F_\beta(i\omega_n,\boldsymbol{k})$ as

$$\Delta_\alpha(\boldsymbol{k}) = -T\sum_{n,\beta,\boldsymbol{k}'} V_{\alpha\beta}(\boldsymbol{k},\boldsymbol{k}') F_\beta(i\omega_n,\boldsymbol{k}'), \quad (7)$$

$$F_\beta(i\omega_n,\boldsymbol{k}) = \frac{\Delta_\beta(\boldsymbol{k})}{\omega_n^2 + \xi^2 + |\Delta_\beta(\boldsymbol{k})|^2}. \quad (8)$$

The transition temperature T_c is determined by the linearized gap equation Eq. (7) for the gap amplitude

$$\Delta_\alpha(\varphi,\theta) = \Delta_\alpha \chi(\varphi,\theta), \quad (9)$$

$$\Delta_\alpha = \sum_\beta \lambda_{\alpha\beta}\Delta_\beta \ln\frac{2\gamma\omega_D}{\pi T_c}, \quad (10)$$

where

$$\lambda_{\alpha\beta} \equiv -V_{\alpha\beta}\nu_\beta, \quad (11)$$

while the eigenvector Δ_β corresponding to the largest eigenvalue of the interaction matrix $\lambda_{\alpha\beta}$ determines the ratios between gaps on different Fermi surfaces set at T_c. Here ν_β are the densities of states (DOSs) per one spin direction for various Fermi surfaces. While the system of gap equations Eq. (7) seems to give a temperature-dependent ratio for gaps on different Fermi surfaces, this result would violate the BCS logarithmic approximation. Within the logarithmic accuracy, the ratios between the gaps on different Fermi surfaces is set at T_c from Eq. (10), and is a temperature-independent constant set by the interaction matrix Eq. (11), the highest-eigenvalue gap eigenvector.[3,4] Then the multiband problem can be parameterized in terms of T_c and the gap ratios, similar to how this is done in the single-band BCS model. An additional related difficulty comes from the fact that the kernel for the system of Fredholm integral equations Eq. (7) is asymmetric, i.e., $\lambda_{\alpha\beta} \neq \lambda_{\beta\alpha}$ for $\nu_\alpha \neq \nu_\beta$. Generalizing the approach of Pokrovskii[75] and following Geilikman *et al.*,[3] we introduce new variables and a symmetric kernel $\mu_{\alpha\beta}=\mu_{\beta\alpha}$,

$$\zeta_\alpha = \sqrt{\nu_\alpha}\Delta_\alpha, \quad (12)$$

$$\mu_{\alpha\beta} = -\sqrt{\nu_\alpha} V_{\alpha\beta} \sqrt{\nu_\beta}. \quad (13)$$

As usual, the gap equation in terms of the universal scale T_c can be obtained by subtracting Eq. (10) from Eq. (7). Writing the result in new variables, we find

$$T\sum_{\beta n} \int d\xi \mu_{\alpha\beta}\zeta_\beta \left[\left\langle \frac{|\chi(\varphi,\theta)|^2}{\omega_n^2 + \xi^2 + |\Delta_\beta|^2|\chi(\varphi,\theta)|^2} \right\rangle_\Omega - \frac{1}{\omega_n^2 + \xi^2} \right] = \sum_\beta \mu_{\alpha\beta}\zeta_\beta \ln\left[\frac{T}{T_c}\right]. \quad (14)$$

Let us now multiply Eq. (14) by ζ_α, and sum over α, using the symmetry of $\mu_{\alpha\beta}$ and Eq. (10),

$$\sum_\alpha \zeta_\alpha \mu_{\alpha\beta} = \sum_\alpha \mu_{\beta\alpha}\zeta_\alpha = \frac{\zeta_\beta}{\ln\frac{2\gamma\omega_D}{\pi T_c}}. \quad (15)$$

The gap equation is then considerably simplified, and can be written in the universal form

$$T\sum_{\beta n} \int d\xi u_\beta^2 \left[\left\langle \frac{|\chi(\varphi,\theta)|^2}{\omega_n^2 + \xi^2 + |\Delta_\beta|^2|\chi(\varphi,\theta)|^2} \right\rangle_\Omega - \frac{1}{\omega_n^2 + \xi^2} \right] = \ln\left[\frac{T}{T_c}\right]. \quad (16)$$

Here

$$u_\beta^2 = \frac{\zeta_\beta^2}{\sum_\alpha \zeta_\alpha^2} = \frac{\nu_\beta\Delta_\beta^2}{\sum_\alpha \nu_\alpha \Delta_\alpha^2} \quad (17)$$

are constant ratios, determined by the gap eigenvector at T_c and the corresponding densities of states. The coefficients u_β are automatically normalized as

$$\sum_\beta u_\beta^2 = 1. \quad (18)$$

As demonstrated in the above derivation, all physical properties in the multiband BCS model can be expressed in terms of the transition temperature T_c, the relevant DOS, and temperature-independent gap amplitudes. The gap ampli-

tudes themselves, however, are not universal. The ratios of the gaps on different Fermi surfaces are nonuniversal constants, determined by the relevant interaction matrix [the highest-eigenvalue eigenvector for $\lambda_{\alpha\beta}$ in Eq. (10)]. Equation (16) can be easily solved at $T=0$. Introducing the usual normalization for the gap,

$$\Delta_{\mathrm{BCS}} = \frac{\pi T_c}{\gamma} e^{-\langle |\chi(\varphi,\theta)|^2 \ln|\chi(\varphi,\theta)|\rangle}, \tag{19}$$

and defining t_α as

$$\Delta_{\alpha 0} \equiv t_\alpha \Delta_{\mathrm{BCS}}, \tag{20}$$

we find

$$\sum_\alpha u_\alpha^2 \ln t_\alpha = 0, \tag{21}$$

which sets a constraint on the amplitude of the gap eigenvector at $T=0$. Equation (19) gives a standard expression for the zero-temperature amplitude of the energy gap for any single-band BCS superconductor. For example,

$$\Delta_{\mathrm{BCS}} = \frac{\pi T_c}{\gamma} \simeq 1.76 T_c, \quad s \text{ wave}, \tag{22}$$

$$\Delta_{\mathrm{BCS}} = \frac{\sqrt{2}\pi T_c}{\gamma\sqrt{e}} \simeq 1.51 T_c, \quad d \text{ wave}. \tag{23}$$

Note that due to the normalization condition Eq. (4), our definition for the d-wave gap amplitude is different from the standard definition by a factor of $\sqrt{2}$. The temperature dependence of the gap amplitude $\Delta(T)$ is determined by the universal gap equation Eq. (16). For the general case multiband case it differs from the single-band BCS temperature dependence as

$$\ln\frac{T}{T_c} = \sum_\alpha \sum_{n=0}^{\infty} u_\alpha^2 \left[\left\langle \frac{|\chi(\varphi,\theta)|^2}{\sqrt{(n+0.5)^2 + (t_\alpha \Delta(T)/2\pi T)^2 |\chi(\varphi,\theta)|^2}} \right\rangle_\Omega - \frac{1}{n+0.5} \right]. \tag{24}$$

Since the ratios of the gaps on different Fermi surfaces are set at T_c, one can obtain thermodynamic potential integrating the gap equation Eq. (24) over the single coupling constant, T_c,

$$\Omega_S - \Omega_N = -\int_0^{T_c} \frac{dT_c'}{T_c'} \sum_\alpha \nu_\alpha \Delta_\alpha^2 \left(\frac{T}{T_c'}\right). \tag{25}$$

Thermodynamics is then given by a sum of standard weak-coupling expressions for separate bands expressed in terms of temperature-dependent energy gaps $\Delta_\alpha(T)$ as follows:

$$\Omega_S - \Omega_N = -\pi T \sum_{\alpha,n} \nu_\alpha \left\langle \sqrt{\omega_n^2 + \Delta_\alpha^2 |\chi(\varphi,\theta)|^2} + \frac{\omega_n^2}{\sqrt{\omega_n^2 + \Delta_\alpha^2 |\chi(\varphi,\theta)|^2}} - 2|\omega_n| \right\rangle_\Omega. \tag{26}$$

Integrating the above expression over ω at zero temperature, one finds the familiar[3] factorized result for the ground-state energy as

$$E_S - E_N = -\sum_\alpha \frac{\nu_\alpha \Delta_{\alpha 0}^2}{2} \langle |\chi(\varphi,\theta)|^2 \rangle_\Omega = -\Delta_{\mathrm{BCS}}^2 \sum_\alpha \frac{\nu_\alpha t_\alpha^2}{2}, \tag{27}$$

where we have used the normalization condition for $\chi(\varphi,\theta)$ given by Eq. (4). The multiband gap equation does produce overall change for the relevant quantities, such as, for example, specific-heat jump at transition temperature, T_c, obtained, for example, in Ref. 3,

$$\frac{\Delta C}{C} = \frac{12}{7\zeta(3)\sum_\alpha \nu_\alpha} \frac{\sum_\alpha \nu_\alpha \Delta_\alpha^4}{(\sum_\alpha u_\alpha^2 \Delta_\alpha^2)^2} = \frac{12}{7\zeta(3)\sum_\alpha \nu_\alpha} \frac{(\sum_\alpha \nu_\alpha \Delta_\alpha^2)^2}{\sum_\alpha \nu_\alpha \Delta_\alpha^4}. \tag{28}$$

The above result of Geilikman *et al.*[3] is applicable to any anisotropic or unconventional superconductors belonging to a one-dimensional representation of the point group,[76,77] which includes d-wave multiband superconductors. For superconductors belonging to a degenerate representation of the point group, the corresponding generalized formula is given by

$$\frac{\Delta C}{C} = \left[\frac{\Delta C}{C}\right]_{\mathrm{BCS}} \frac{1}{\sum_\alpha \nu_\alpha} \frac{(\sum_\alpha \nu_\alpha \Delta_\alpha^2)^2}{\sum_\alpha \nu_\alpha \Delta_\alpha^4}, \tag{29}$$

where $[\Delta C/C]_{\mathrm{BCS}}$ is the weak-coupling value of the specific-heat jump at T_c for a given multiband representation, given, for example, by Kuznetsova and the author in Ref. 78.

As a simple example, let us consider the two-band case. The expression for the constant ratio of the energy gaps on different Fermi surfaces is then very easily obtained from Eq. (10) in terms of the interaction constants Eq. (11) (also see, for example, Ref. 23),

$$\frac{\Delta_2(T)}{\Delta_1(T)} = \frac{\Delta_2(T_c)}{\Delta_1(T_c)} = \frac{2\lambda_{12}}{\lambda_{22} - \lambda_{11} + \sqrt{(\lambda_{11} - \lambda_{22})^2 + 4\lambda_{12}\lambda_{21}}} \equiv s. \tag{30}$$

The other relevant parameter of the BCS model is u_1^2, defined by Eq. (17),

$$u_1^2 = \frac{\nu_1}{\nu_1 + \nu_2 s^2} = 1 - u_2^2. \tag{31}$$

Since the gaps on all Fermi surfaces have the same temperature dependence, let us introduce a normalized gap amplitude Δ as given by Eq. (20),

$$\Delta_\alpha(T) = t_\alpha \Delta(T), \quad \Delta(T=0) = \Delta_{\mathrm{BCS}}. \tag{32}$$

We then easily find the expression for zero-temperature gaps on the two Fermi surfaces,

$$t_1 = s^{-u_2^2}, \quad t_2 = s^{u_1^2}. \tag{33}$$

The temperature dependence of the gaps on the two Fermi surfaces must be the same. In addition to T_c, thermodynam-

ics is completely determined by two other parameters, s and u_1, which can be easily found from experiment.

We conclude that the universality of the weak-coupling BCS-like model is applicable to the multiband case. However, some nonuniversal constants, which depend on the interactions, do enter the problem as temperature-independent parameters. The total number of independent parameters for an m-band BCS model is then significantly reduced to $2m-1$ measurable constants: T_c, $m-1$-independent constant DOS ratios ν_α/ν_β, and $m-1$-independent constant gap ratios $\Delta_\alpha/\Delta_\beta$. A significant temperature dependence of the energy gap ratios on different Fermi surfaces as, for example, observed in MgB_2, then corresponds to the failure of the weak-coupling logarithmic approximation.

III. PARTIAL GAPLESS STATE IN MAGNETIC FIELD IN *S*-WAVE SUPERCONDUCTORS

In this section we consider the unbalanced pairing problem[41,42] for a multiband s-wave superconductor placed in paramagnetic magnetic field. The author and Gor'kov[71] recently showed that a stable gapless state appears in small magnetic fields. The emergence of this state for s-wave superconductors is accompanied by zero-temperature first-order phase transition. The s-wave case can be solved analytically at $T=0$. In what follows, we present our results for the stability of the gapless state in s-wave multiband superconductors and the details of the B-T phase diagram.

A. Nature of the gapless state

We start by considering the general solution for the BCS gap equation for a multiband superconductor placed in magnetic field. We neglect the diamagnetic effects (H_{c2}). The presence of paramagnetic magnetic field results in an additional Pauli term in the Hamiltonian for each separate band,

$$H_p = -\frac{1}{2}\sum_{\mathbf{k}ij\alpha} g_\alpha a^\dagger_{\alpha i}(\mathbf{k})(\boldsymbol{I}\cdot\boldsymbol{\sigma}_{ij})a_{\alpha j}(\mathbf{k}), \quad \boldsymbol{I}\equiv\mu_B\boldsymbol{B}. \tag{34}$$

Here g_α is the g factor for each band α, taken to be isotropic in this section. The multiband gap equations in magnetic field have the same form Eq. (7), with the Gor'kov function F given by

$$\hat{F}_\alpha(\omega_n,\mathbf{p}) = \frac{-i\hat{\sigma}^y\Delta_k(\mathbf{p})}{(i\omega_n - I\hat{\sigma}^z)^2 - \xi_\alpha(\mathbf{k})^2 - |\Delta_\alpha(\mathbf{p})|^2}. \tag{35}$$

The diagonalization procedure of Pokrovskii[75] and Geilikman *et al.*[3] is applicable in the presence of arbitrary magnetic field, i.e., the ratios of the gaps on different Fermi surfaces do not change as functions of both temperature and magnetic field, and are determined by the gap eigenvector at T_c. For example, Eq. (30) for the two-band problem in the presence of magnetic field[71] can be written as

$$s \equiv \frac{\Delta_2(T,B)}{\Delta_1(T,B)} = \frac{\Delta_2(T_{c0})}{\Delta_1(T_{c0})} = \frac{2\lambda_{12}}{\lambda_{22}-\lambda_{11}+\sqrt{(\lambda_{11}-\lambda_{22})^2+4\lambda_{12}\lambda_{21}}}, \tag{36}$$

where $T_{c0}=T_c(B=0)$.

Thus, as it is the case with the energy gaps and thermodynamics, it is possible to obtain a complete solution of the multiband problem in magnetic field in terms of T_c, gap ratios, and DOS ratios. The linearized gap equations in magnetic field produce the instability curve $T_c(B)$, which takes the following form:

$$\ln\frac{T_c}{T_{c0}} = \Psi\left(\frac{1}{2}\right) - \sum_\alpha u_\alpha^2 \mathrm{Re}\left[\Psi\left(\frac{1}{2}+i\frac{g_\alpha I}{4\pi T_c}\right)\right], \tag{37}$$

where u_α are band-dependent constants given by Eq. (17). Note that in the free-electron case, $g_\alpha=2$, the multiband instability curve Eq. (37) is reduced to the familiar single-band result, in agreement with earlier results,[71]

$$\ln\frac{T_c}{T_{c0}} = \Psi\left(\frac{1}{2}\right) - \mathrm{Re}\left[\Psi\left(\frac{1}{2}+i\frac{I}{2\pi T_c}\right)\right]. \tag{38}$$

The re-entrant behavior of T_c with increased magnetic field normally indicates the possibility of first-order phase transitions on the B-T phase diagram. In a single-band problem the homogeneous gap equation gives rise to a second unstable solution[59] in magnetic fields close to the paramagnetic limit, also known as the Sarma[43] state. The instability is resolved in favor of an inhomogeneous LOFF (Refs. 41 and 42) state. As we have shown in the recent letter,[71] in the two-band case one has three different solutions. In the general m-band case, the number of solutions will be $m+1$. The $T=0$ solution of the gap equation will change form at $I=\Delta_\alpha(B)$. For the s-wave case all solutions can be written out analytically as

$$\prod_{\alpha, g_\alpha I>2\Delta_\alpha(I)} \left(\frac{\sqrt{(g_\alpha I)^2-4\Delta_\alpha(I)^2}+g_\alpha I}{2\Delta_{\alpha 0}}\right)^{u_\alpha^2} \times \prod_{\alpha, g_\alpha I<2\Delta_\beta(I)} \left(\frac{\Delta_\beta(I)}{\Delta_{\beta 0}}\right)^{u_\beta^2} = 1. \tag{39}$$

Here α and β are band indices, u_α^2 are given by Eq. (17), while $\Delta_{\alpha 0}$ correspond to the solution of the multiband gap equation at $T=0$ without the magnetic field, Eq. (20). Stability of these solutions can be inferred from the ground-state energy, which can be easily obtained by the integration of the gap equation over the coupling constant T_c, as in Eq. (25),

$$E_S - E_{N0} = -\sum_\alpha \frac{\nu_\alpha \Delta_\alpha(I)^2}{2} - \frac{1}{4}\sum_{\beta, g_\beta I>2\Delta_\beta(I)} \nu_\beta g_\beta I\sqrt{(g_\beta I)^2-4\Delta_\beta(I)^2}. \tag{40}$$

Here E_{N0} is the normal-state energy in the absence of magnetic field.

We can also write out the solution of the multiband gap equation at finite temperatures since there is only a single temperature and field-dependent variable, the same for all $\Delta_\alpha(T,B)$,

$$\delta(T,B) \equiv \frac{\Delta_\alpha(T,B)}{\Delta\alpha(T=0,B=0)}. \tag{41}$$

The gap equation then takes a simple form

$$\ln[\delta(T,B)] = \sum_{\alpha} u_{\alpha}^2 f_0\left(\frac{\Delta_\alpha(T,B)}{T}, \frac{g_\alpha I}{2T}\right), \tag{42}$$

where

$$f_0(x,y) = \int_0^\infty \frac{dt}{\sqrt{t^2+x^2}}\left(\frac{\sinh(\sqrt{t^2+x^2})}{\cosh(y)+\cosh(\sqrt{t^2+x^2})} - 1\right), \tag{43}$$

which is the same function that appears in the single-band model. The expression for thermodynamic potential in magnetic field is an analytic continuation of the corresponding expression in zero field to $i\tilde{\omega}_n = i\omega_n - (g_\alpha I/2)$, which is also factorizable

$$\Omega_S - \Omega_N(I) = -\frac{1}{2}\sum_{\alpha} \nu_\alpha |\Delta_\alpha(B,T)|^2\left(1 + f_1\left[\frac{\Delta_\alpha(B,T)}{T}, \frac{g_\alpha I}{2T}\right]\right), \tag{44}$$

with

$$f_1(x,y) = \frac{1}{2x^2}\int_0^\infty t^2 dt\left(\cosh^{-2}\left[\frac{\sqrt{t^2+x^2}-y}{2}\right] + \cosh^{-2}\left[\frac{\sqrt{t^2+x^2}+y}{2}\right] - \cosh^{-2}\left[\frac{t-y}{2}\right] - \cosh^{-2}\left[\frac{t+y}{2}\right]\right). \tag{45}$$

Here

$$\Omega_N(I) = \Omega_{N0} - \frac{1}{4}\sum_{\alpha} \nu_\alpha (g_\alpha I)^2 \tag{46}$$

is the normal-state energy in exchange magnetic field I.

From the general analysis of Eq. (40) one can see that the solution with $g_\alpha I > 2\Delta_\alpha(I)$ for all α is always unstable, similar to the unstable Sarma state of the single-band problem.[59] The low-field solution, $g_\alpha I < 2\Delta_\alpha(I) = 2\Delta_{\alpha 0}$ for all α, on the other hand, corresponds the multiband BCS solution at $I=0$, which is stable in low enough magnetic fields. The other solutions of the gap equation correspond to partial Sarma states, illustrated on Fig. 1 for the two-band case and $g_\alpha = 2$. The energy spectrum of the system for excitations near each Fermi surface (FS) is given by the poles of the Green's function $\hat{G}_\alpha(\omega_n, \boldsymbol{k})$,

$$\hat{E}_\alpha(\boldsymbol{k}) = \sqrt{\xi_\alpha(\boldsymbol{k})^2 + |\Delta_\alpha(\boldsymbol{k})|^2} + \frac{1}{2} g_\alpha I \sigma^z. \tag{47}$$

As the magnetic field exceeds the value of the smallest gap, a strip of unpaired fully polarized quasiparticles forms in the vicinity of the corresponding Fermi surface, giving rise to a paramagnetic magnetic moment. Similar to the single-band problem, the LOFF state competes with homogeneous solutions in high magnetic fields. A generalization of the instability curve Eq. (37) can be written for an arbitrary inhomogeneous q vector as

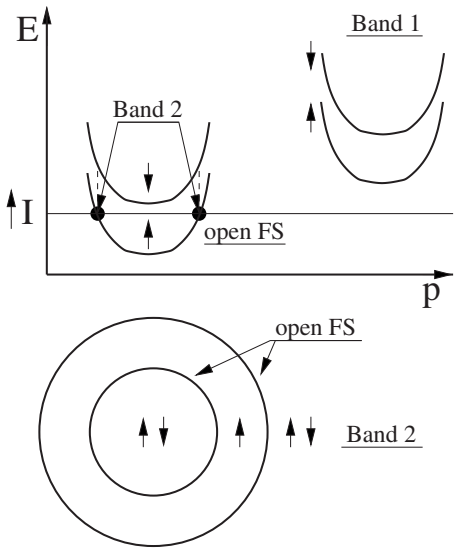

FIG. 1. Multiband partial Sarma state at $T=0$, characterized by fully polarized unpaired electrons near the Fermi surface of the driven band. The state is stabilized by the presence of the gap on the primary Fermi surface.

$$\ln\frac{T_c}{T_{c0}} = \Psi\left(\frac{1}{2}\right) - \sum_{\alpha} u_\alpha^2 \left\langle \mathrm{Re}\left[\Psi\left(\frac{1}{2} + i\frac{g_\alpha I + 2(\boldsymbol{v}_{F\alpha}\boldsymbol{q})}{4\pi T_c}\right)\right]\right\rangle, \tag{48}$$

where $\boldsymbol{v}_{F\alpha}$ is the Fermi velocity for band α. $T_c(I)$ is then found as a maximum with respect to $\boldsymbol{q}$. The high-field phase transition is always second order. As the field is lowered, the regions of stability of various phases and the exact nature of the LOFF state in the general case, when the energy gaps are of the same order of magnitude, can only be obtained numerically.

The zero-temperature phase transition in partially gapless state in s-wave multiband superconductors is accompanied by the appearance of the paramagnetic moment.[71] In non-s-wave multiband superconductors, however, magnetic moment is always present in low magnetic fields due to the nodes in the energy spectrum. The transition to partial Sarma state then corresponds to a crossover from the nodal regime to a regime with a full open Fermi surface. In completely isotropic situation, the zero-temperature phase transition to partial Sarma state in s-wave superconductors is always first order, corresponding to the appearance of a finite paramagnetic magnetic moment. Effects of spin-orbit, nonspherical Fermi surface, or gap anisotropy can turn this phase transition into a smooth crossover. Similarly, due to effects of gap anisotropy, the first-order zero-temperature phase transition in multiband d-wave superconductors exists only in a certain region of parameters.[71] The first-order phase transition, if present, disappears above a certain critical temperature, T_{cr}.

The analysis of the B-T phase diagram for multiband superconductors depends on the same number of parameters as the analysis of other properties considered in Sec. II. Thus, for example, energetic stability of various gapless state will depend on the value of these additional parameters. We thus consider for simplicity a two-band model, which has only

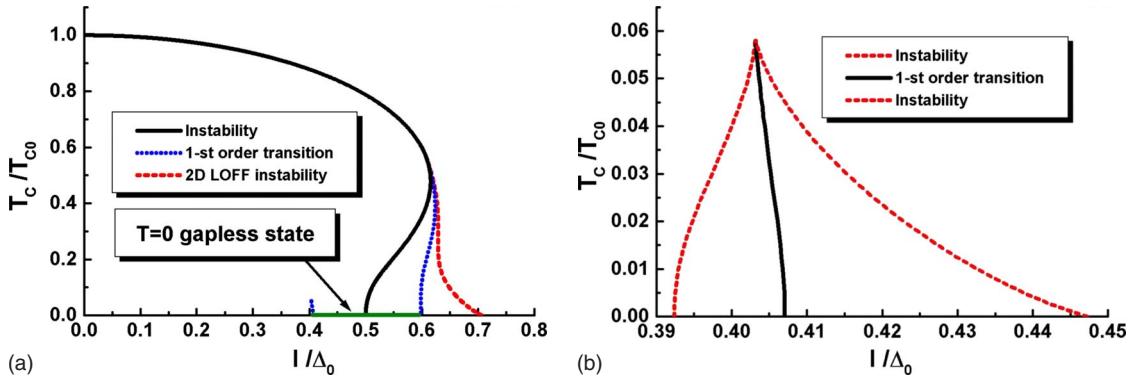

FIG. 2. (Color online) (a) B-T phase diagram for a 2D two-band superconductor with two equal circular Fermi surfaces ($p_{F1}=p_{F2}$) and $(\Delta_2/\Delta_1)=0.2$, $(m_2/m_1)=25$. The dotted blue line corresponds to the first-order phase transition into the partial Sarma state from the normal state (right side, the Clogston limit) or fully gapped superconducting state (left side). The LOFF instability is shown by a dashed red line. The instability for the normal/uniform superconducting state is shown by the solid black line. (b) Details of low-temperature first-order transition from fully gapped to gapless superconducting state. The black line marks the first-order phase transition. The red dashed lines correspond to the boundaries of the region of metastable states, where the hysteretic behavior is expected to occur.

two additional physical constants, the ratio of the densities of states on two Fermi surfaces, ν_2/ν_1, and the ratio of the energy gaps Δ_2/Δ_1. We also assume for simplicity $g_1=g_2=2$ and only consider homogeneous solutions since the LOFF state will depend on the shape of both Fermi surfaces. Figure 2(a) shows an example B-T phase diagram for homogeneous phases for the two-band isotropic s-wave model in exchange field and parameters $(\Delta_2/\Delta_1)=0.2$ and $(\nu_2/\nu_1)=25$ obtained with the help of the above expressions for the temperature-dependent gaps and thermodynamic potential Ω_S. The instability line in Fig. 2(a) for the transition into a uniform partially gapless superconducting state has the characteristic reversal behavior, which indicates the presence of either a LOFF state[41,42] or a first-order phase transition. The LOFF instability line for two equal circular Fermi surfaces with different masses in two dimensions is shown by the red dashed line. When only the uniform superconducting states are considered, the partially gapless state will be separated from the normal state in high magnetic field and low temperatures by a first-order Clogston-type transition. At low fields it is separated from the fully gapped superconducting state by a first-order line that ends in a critical point. Figure 2 shows the details of the first-order phase transition from fully gapped superconducting state to partially gapless superconducting state. The first-order transition is shown by the solid black line that ends in a critical point at $T=T_{\mathrm{CR}}\simeq 0.058T_{c0}$. The dashed red lines mark the boundaries metastable region in the vicinity of the first-order phase transition where unstable solutions of the gap equation are present.

Figure 3 shows the solution of the multiband gap equation Eq. (42) as a function of temperature and magnetic field. The unusual reversal behavior of the energy gap reflects the presence of a first-order phase transition. While there are three different solutions at a given field in a region near this phase transition, only one of these solutions is stable. Such a region corresponds to the region of the first-order phase transition where the hysteresis exists. The stable solution corresponds to the minimum of the Free energy, Eq. (44), shown in Fig. 4. The shape of the Gibbs Free energy at $T<T_{\mathrm{cr}}=0.058T_{c0}$ also reflects the presence of the metastable states near the first-order phase transition into the gapless superconducting state. The system always picks the lowest energy. Thus, the free energy of the system as a function of magnetic field has a slope change at the point of first-order phase transition, where the energy gap and paramagnetic magnetization have a corresponding jump.

The zero-temperature phase transition into the state is characterized by a metamagnetic jump of magnetization. At $T=0$ the magnetic moment appears sharply, from $M=0$ to $M\neq 0$. At a finite temperature small magnetization is present due to thermal population of the band with smaller energy gap. The first-order phase transition line disappears at $T>T_{\mathrm{cr}}$, as the quasiparticle states above the gapless state become thermally populated. Thus, one has two metamagnetic transitions shown in Fig. 3, one corresponding to the transition into partially gapless Sarma state, the other is the first-order phase transition from the partially gapped Sarma state into the normal state.

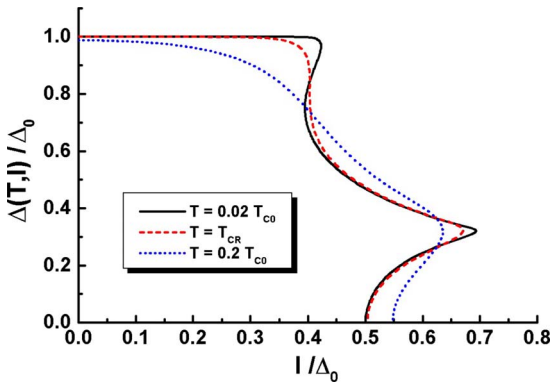

FIG. 3. (Color online) Numerical solution of the two-band BCS gap equation $\Delta(T,B)$ at different temperatures for parameters in Fig. 2. Three solutions for the gap equation at low fields and temperatures reflect the existence of unstable region near the first-order phase transitions from fully gapped state into partially gapless state. As the temperature is raised above the critical temperature, the first-order region disappears, and there is only one solution for the gap equation in low fields. The high-field behavior corresponds to the usual first-order unstable Clogston limit.

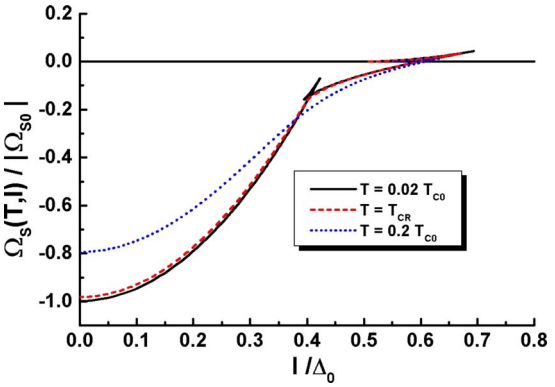

FIG. 4. (Color online) Free energy Ω_S of the superconducting state for a two-band superconductor in magnetic field at different temperatures for the parameters in Fig. 2. The reversal behavior at low temperatures $T<T_{\rm cr}=0.058T_{c0}$ indicates the presence of the first-order phase transition from the fully gapped superconducting state into a partially gapless gapless superconducting state. The first-order transition from the partially gapped superconducting state to normal state in high magnetic fields happens at the point when the condensation energy $\Omega_S(T,I)=0$.

The analysis of the above equations can be done numerically for any parameters ν_2/ν_1 and Δ_2/Δ_1. For the *s*-wave case, however, analytical results for the energy and the magnetic moment can be obtained at $T=0$. In a special case when the critical point is located at low enough temperatures, the critical region is fully determined by the second Fermi surface and depends only on one energy scale. We consider these simplified results below.

Finally, we note that the partial gapless state is not always present on the *B*-*T* phase diagram; for some parameters of the two-band model, as shown below, the first-order transition happens directly from the uniform superconducting state into the normal state.

B. Magnetic properties of the partial gapless state at $T=0$

In this section we consider the low-field transition to partial gapless state. As we have seen in Sec. III A, the gap equation for the two-band model has three different solutions and depends on two constant parameters, the ratio of the energy gaps on the two Fermi surfaces *s*, determined only by interactions, Eq. (36), and the ratio of the densities of states for the two bands. However, analytical expressions are more conveniently written in terms of *s* and a combination of these parameters u_2^2, defined in Eq. (31).

The uniform low-field solution at $T=0$ is the same as the solution without the magnetic field. The first-order phase transition appears near $I\simeq\Delta_{20}$. It is thus convenient to rewrite the solution in terms of Δ_{20} and other parameters of the second Fermi surface. For example, the energy of the superconducting state at $T=0$ and $B=0$ is

$$E_{s0}=-\frac{1}{2u_2^2}\nu_2\Delta_{20}^2. \tag{49}$$

Introducing

$$\tilde{\Delta}\equiv\frac{\Delta_2(B,T)}{\Delta_{20}}=\frac{\Delta_1(B,T)}{\Delta_{10}}, \tag{50}$$

$$\tilde{I}\equiv\frac{I}{\Delta_{20}}, \tag{51}$$

we find a simple expression for I in the partially gapped state as

$$\tilde{I}=\frac{1}{2}\tilde{\Delta}(\tilde{\Delta}^{u_2^{-2}}+\tilde{\Delta}^{-u_2^{-2}}), \tag{52}$$

or

$$\tilde{I}=\tilde{\Delta}\cosh(u_2^{-2}\ln\tilde{\Delta}). \tag{53}$$

The expression for the energy also simplifies to

$$\frac{E_S}{E_{S0}}=\tilde{\Delta}+2u_2^2\tilde{I}\sqrt{\tilde{I}^2-\tilde{\Delta}^2}. \tag{54}$$

The first-order transition point is determined from the smallest $\tilde{\Delta}<1$ solution of the transcendental equation,

$$1-u_2^2\sinh(2u_2^{-2}\ln\tilde{\Delta}_{\rm cr})=\tilde{\Delta}_{\rm cr}^{-2}, \tag{55}$$

where the solution changes abruptly from $\tilde{\Delta}=1$ to the smaller gap branch of Eq. (53). The magnetization in the partial Sarma state as a function of $\tilde{\Delta}$ is also easily determined since it is also just a fraction of the normal-state magnetization on the second Fermi surface,

$$M=-2\mu_B\nu_2 I\tanh(u_2^{-2}\ln\tilde{\Delta}). \tag{56}$$

Equations (53) and (56) determine the field dependence of magnetization in the partial gapless state parametrically. Magnetization has a jump from 0 to a finite value at the first-order phase transition $\tilde{\Delta}_{\rm cr}$. The transition point can be easily found analytically in a particular case of $u_2^2\ll 1$, corresponding to "induced" superconductivity on the second Fermi surface.[71] Indeed, introducing

$$\tau_\Delta\equiv\tilde{\Delta}-1, \tag{57}$$

Eq. (53) transforms to

$$\tau_I=\frac{1}{2}\frac{\tau_\Delta^2}{u_2^4}+\tau_\Delta, \tag{58}$$

while for the condensation energy we easily find the following expression:

$$\frac{E_S}{E_{S0}}=1-2\tau_\Delta^2-\frac{4}{3u_2^4}\tau_\Delta^3, \tag{59}$$

The cubic terms in the energy lead to a first-order phase transition[71] at

$$\tau_{I\rm cr}=-3u_2^4/8, \tag{60}$$

where the energy gap τ_Δ changes abruptly from $\tau_\Delta=0$ to $\tau_\Delta=-3u_2^4/2$. The magnetization changes abruptly at $\tau_{I\rm cr}$ from zero to

$$M_{\rm cr} = \frac{3}{2} u_2^2 \mu_B \nu_2 \Delta_{20}. \quad (61)$$

C. High-field Clogston limit and energetic stability of the gapless state at $T=0$

We now turn to the first-order transition in high magnetic field, or the modification for the Clogston criterion for the two-band model. The standard Clogston Criterion involves a transition from the uniform superconducting state to the normal state, determined by

$$E_{S0} = -\frac{\nu_1 \Delta_{10}^2}{2} - \frac{\nu_2 \Delta_{20}^2}{2} = E_N(I) = -(\nu_1 + \nu_2) I_{\rm clog}^2. \quad (62)$$

We thus obtain

$$I_{\rm clog} = \frac{1}{\sqrt{2}} \sqrt{\frac{\nu_1 \Delta_{10}^2 + \nu_2 \Delta_{20}^2}{\nu_1 + \nu_2}} \quad (63)$$

The transition first-order transition from gapped two-band superconductor to the normal state only happens at $I=I_{\rm clog}$ in the absence of the partially gapless state. Since the partially gapless state is different from the uniform gapped state, the high-field transition to the normal state will also happen in a different magnetic field, now determined by

$$E_S(I) = E_N(I). \quad (64)$$

After simple calculations, we find

$$\tilde{\Delta}_{{\rm clog}\ 1}^{2u_2^{-2}} = \frac{u_1 s^2}{u_1(1-s^2) + \sqrt{u_1^2 - 2s^2}}, \quad (65)$$

where $u_1 = \sqrt{1-u_2^2}$, and the new Clogston limit $I_{{\rm clog}\ 1}$ then determined by Eq. (53) that connects $\tilde{\Delta}$ and I in the partially gapless state.

It is obvious that the condition

$$I_{{\rm clog}\ 1} > I_{\rm cr}, \quad (66)$$

where $I_{\rm cr}$ is the magnetic field for the $T=0$ transition from uniform into partially gapless state must be met for the partially gapless state to be present on the phase diagram. In particular, it is obvious that for

$$s > \frac{u_1}{\sqrt{2}} \quad (67)$$

the partially gapless state is definitely not present. The accurate condition is given by Eq. (66), which upon substitution of Eq. (65) into Eq. (55) takes the following form:

$$1 - u_2^2 \sinh(2u_2^{-2} \ln \tilde{\Delta}_{{\rm clog}\ 1}) > \tilde{\Delta}_{{\rm clog}\ 1}^{-2}. \quad (68)$$

The region of parameters of the two-band model where the partially gapless state exists given by Eq. (68) is shown in Fig. 5. We see that in order for the gapless state to be present and easily observable, the second gap has to be much smaller than the first gap, while the density of states on the second Fermi surface should be quite a bit larger than on the first one, otherwise the entropy change associated with the first-order transition will be very small and not easily detectable. Such transition will also be turned into a crossover in the presence of even small gap anisotropy, impurities, nonzero temperature, or other effects.[79]

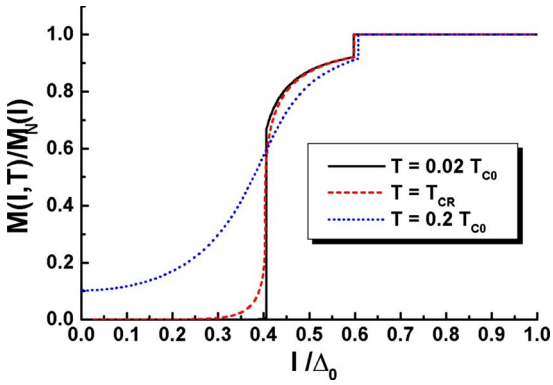

FIG. 5. (Color online) The region of parameters for the two-band model for which the $T=0$ gapless phase is present.

We have not considered the details of the high-field stripe LOFF (Refs. 41 and 42) region beyond the LOFF instability in the normal state given by Eq. (48) and shown in Fig. 2, since this calculation depends on the details of the shape of the Fermi surfaces, their dimensionality, and thus a number of additional parameters.[80] Unlike the Clogston limit, the LOFF region is very nonuniversal and sensitive to defects. We note, however, that the LOFF stripe phase will also be unusual since it forms in high enough magnetic fields in the vicinity of the first-order transition between partially gapless state and the normal state. In particular, the inhomogeneous LOFF state will likely involve superconducting stripe order made out of the partially gapless state. It is also not completely clear whether the phase transitions between the partially gapless superconducting state and the LOFF state and between the LOFF state and the normal state will be first or second order.

D. Low-field critical region

The mathematics of the low-field critical region near the $T=0$ first-order phase transition into the partially gapless superconducting state and the associated thermodynamics is rather bulky, and can only be studied numerically for the general case (see Figs. 2–4 and 6). Nevertheless, as it was shown in Secs. III A–III C, *only parameters for the second Fermi surface* are relevant for the first-order phase transition at $T=0$. Unfortunately, *both* Fermi surfaces determine the critical region at finite temperatures. However, when $u_2^2 \ll 1$, the critical region lies at very low temperatures, and thus only the quasiparticle excitations near the gapless or nearly gapless state on the second Fermi surface are important. The results for the critical region then depend only on parameters of the second Fermi surface only, and thus it can be found in a universal form. We note that the special case $u_2^2 \ll 1$, corresponding to superconductivity driven by a single Fermi surface and induced by interactions on other Fermi surfaces is, perhaps, most common for multiband superconductors. In this section we consider such a weak first-order transition,

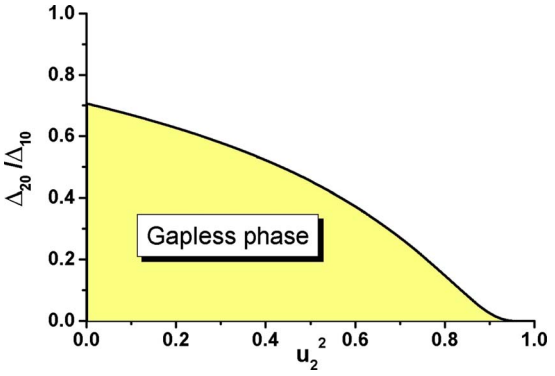

FIG. 6. (Color online) Magnetic moment normalized to magnetic moment in the normal state at different temperatures for the parameters in Fig. 2. The first-order jump in magnetization from zero to finite magnetic moment in the lower fields and temperatures $T<T_{\rm cr}=0.058T_{c0}$ corresponds to a transition into partially gapless state. The sharp transition is absent at temperatures above the critical temperature, as quasiparticle states above the second smaller gap become thermally populated.

assuming that both Fermi surfaces are completely isotropic.

The $T=0$ first-order phase transition in this limit happens near $I\simeq\Delta_{20}$. To describe this phase transition and thermodynamics near it, following Ref. 71, it is convenient to introduce new dimensionless variables that correspond to deviation of the second energy gap and the magnetic field from Δ_{20},

$$\tau_I \equiv \frac{I-\Delta_{20}}{\Delta_{20}}, \tag{69}$$

$$\tau_\Delta \equiv \frac{\Delta_2(T,I)-\Delta_{20}}{\Delta_{20}}, \tag{70}$$

and dimensionless temperature

$$t \equiv \frac{T}{\Delta_{20}}. \tag{71}$$

The solution for the metamagnetic transition at $T=0$ in this limit is given by Eqs. (58) and (59). It is not difficult to extend this solution to finite temperatures. The gap equation then takes the following form:

$$\tau_\Delta = -u_2^2\sqrt{t}\int_0^\infty \frac{\sqrt{x}dx}{\cosh^2\left[x+\frac{\tau_\Delta-\tau_I}{2t}\right]}. \tag{72}$$

Thermodynamics near the critical point is simply given by the integral of the gap equation,

$$\Omega_S-\Omega_{S0}=4|\Omega_{S0}|\int_{-\infty}^{\tau_I}\tau_\Delta(\tau_I)d\tau_I. \tag{73}$$

The critical point can be found by differentiating Eq. (72) and solving the following two equations:

$$\frac{d\tau_I}{d\tau_\Delta}=\frac{d^2\tau_I}{d\tau_\Delta^2}=0. \tag{74}$$

The critical temperature is given by

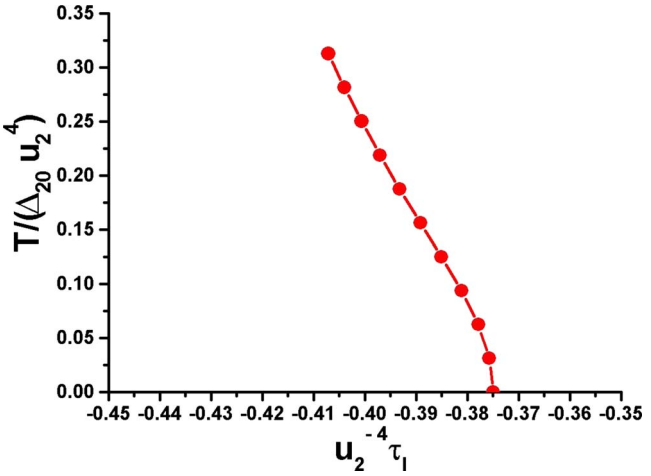

FIG. 7. (Color online) The T-B phase diagram near the first-order transition to partially gapless Sarma state in the special case of weak first-order transition, marked by a red solid line.

$$t_{\rm cr}=A_1^2u_2^4, \tag{75}$$

with

$$A_1 \equiv \int_0^\infty \frac{\sqrt{x}\tanh(x+A_2)dx}{\cosh^2(x+A_2)}, \tag{76}$$

where A_2 is the solution of

$$\int_0^\infty \sqrt{x}dx\frac{1-2\sinh^2(x+A_2)}{\cosh^4(x+A_2)}=0. \tag{77}$$

The energy gap and magnetic field at the critical point are given by

$$\tau_{\Delta,{\rm cr}}=-A_1u_2^4\int_0^\infty \frac{\sqrt{x}dx}{\cosh^2(x+A_2)}, \tag{78}$$

$$\tau_{I,{\rm cr}}=\tau_{\Delta,{\rm cr}}-A_2t_{\rm cr}. \tag{79}$$

Solving for A_1 and A_2 numerically, we obtain

$$t_{\rm cr}=0.3129u_2^4, \tag{80}$$

$$\tau_{\Delta,{\rm cr}}=-0.7541u_2^4, \tag{81}$$

$$\tau_{I,{\rm cr}}=-0.4071u_2^4. \tag{82}$$

It is not difficult to see that the solutions for the gap equation, the energy, and the magnetic moment in the critical region depend on single energy scale $T_{\rm cr}$ or $u_2^4\Delta_{20}$. Thus, universal numerical results for the critical region can be obtained.

In Fig. 7 we show the first-order transition line on the B-T phase diagram in universal units $u_2^{-4}\tau_I$ and $T/(\Delta_{20}u_2^4)$. Figure 8 shows the solution of the gap equation in the critical region at different temperatures in universal units $u_2^{-4}\tau_I$ and $u_2^{-4}\tau_\Delta$. The gap equation has three different solutions. The black line is the line of first-order phase transitions of Fig. 7 in these coordinates. The two τ_Δ on this line at a given field τ_I cor-

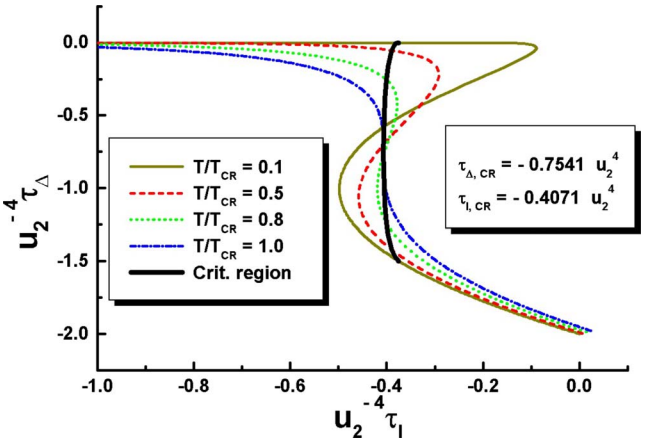

FIG. 8. (Color online) Solution for the gap equation in the low-field critical region as a function of magnetic field and temperature. The black line is the first-order transition line for different temperatures in B-Δ coordinates, also shown in Fig. 7 in B-T coordinates.

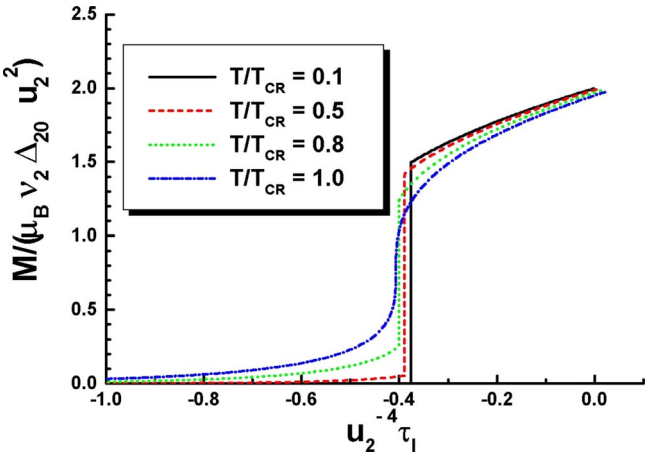

FIG. 10. (Color online) First-order metamagnetic transition into partially gapless state at different temperatures $T<T_{cr}$. The transition disappears and becomes a crossover at $T>T_{cr}$.

respond to the two coexisting superconducting states on the first-order line at a given temperature. The thermodynamic potential $\Omega=(\Omega_S/\Omega_{S0})-1$ is shown in reduced units Ωu_2^{-8} in Fig. 9. The behavior of the gap as a function of magnetic field results, as usual, in the presence of metastable states in the vicinity of the first-order phase transition. Finally, Fig. 10 shows the jump in paramagnetic magnetization at different temperatures below the critical temperature T_{cr} in reduced units of $M/(\mu_B \nu_2 \Delta_{20} u_2^2)$. As the temperature is raised to T_{cr}, the first-order jump disappears.

IV. CONCLUSIONS

Let us now briefly summarize our main results. We have performed a detailed calculation of energetically stable homogeneous superconducting states in the unbalanced pairing problem for s-wave multiband superconductors. Our analysis shows that this problem differs from one for single-band superconductors, and that partially gapless states may be present in the low-temperature region of the B-T phase diagram. These states are characterized by a gapless Fermi spectrum, open Fermi surfaces, and a finite paramagnetic magnetic moment. The phase transition between fully gapped and gapless superconducting states in magnetic field at $T=0$ is a metamagnetic first-order phase transition, which corresponds to a sharp jump in magnetization on one of the Fermi surfaces that becomes gapless.

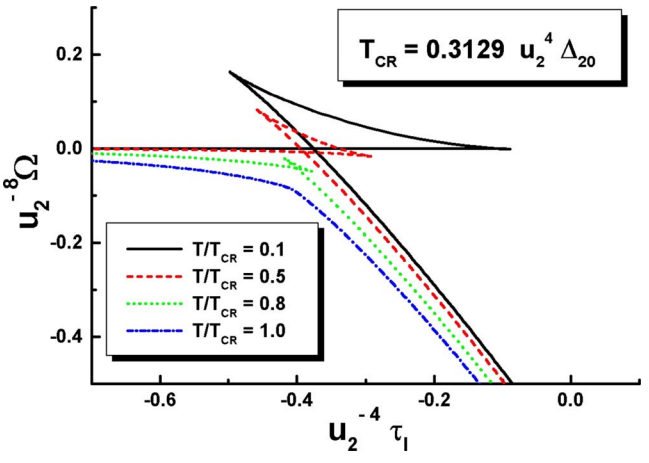

FIG. 9. (Color online) Gibbs free energy of the superconducting state near the first-order phase transition to the partially gapless state for different temperatures $T\leq T_{cr}$. The unusual behavior of the Gibbs potential indicates the presence of metastable states near the first-order transition from fully gapped to partially gapless superconducting state.

The superconducting order is present on both Fermi surfaces, as shown in Fig. 1. At finite low temperatures the metamagnetic first transition results a first-order line on the B-T phase diagram that ends in a critical point, as shown in Fig. 2. The presence of the gapless superconductivity also modifies the high-field Clogston limit. While the state is analogous to the one studied in Ref. 55, it is not the same. Unlike the situation encountered in Bose condensation or high-energy physics, unbalanced pairing of different species of fermions in superconductors is energetically unfavorable because of the large difference of the corresponding Fermi surfaces. Pairing in multiband superconductors is associated with each Fermi surface separately, although the gaps on different Fermi surfaces are related by the interaction. In the weak-coupling logarithmic scheme that ratio is temperature and field independent. Nevertheless, we found that, similar to Ref. 55, the gapless state is most visible when the superconducting gap on the heavier band is driven by the superconducting transition on the lighter band.

Strong anisotropy of the B-T diagram, which indicates a quasi-2D nature of 2H-$NbSe_2$, and its multigap superconductivity[21,20] makes a case for a possible first-order phase transition to a ground state of this type in low magnetic fields parallel to the plane in this material.[71] An unusual first-order phase transition has been indeed observed in this material[81] for thermal-conductivity measurements in low magnetic field $H\sim 10$ kOe$\ll H_{c2}$ parallel to the basal plane. This first-order phase transition is inconsistent with explanations involving vortex lattice melting.[81] The magnetic field at

which this transition occurs is consistent with the value of the small energy gap $\sim 0.1-0.2$ meV observed in the photoemission experiments.[21] The low-field first-order phase transition in $NbSe_2$ was found to be strongly anisotropic, and the hysteretic behavior of thermal conductivity disappears for certain field directions,[81] a behavior not expected in a simple multiband model considered above, where a first-order phase transition occurs for all field directions in the basal plane. However, in the presence of CDW the CI symmetry is broken,[82] which itself has been shown to lead to a strong in-plane anisotropy of the *B-T* phase diagram.[36] Similar effects must be present for the low-field metamagnetic phase transition as well. Gap anisotropy, *g*-factor anisotropy, and spin-orbit coupling tend to wipe out the first-order line on the *B-T* phase diagram, and turn it in a smooth crossover.[71] We have recently found that the order of the phase transition in the presence of spin-orbit interaction may, too, be dependent on direction. As a result of two different terms in the spin-orbit interaction, the first-order phase transition becomes very anisotropic. It is present for some field directions and turns into a smooth crossover for other field directions.[79]

Experimental observation of the gapless state is subject to the usual difficulties associated with the observation of paramagnetic pair breaking and the LOFF state in superconductors. Namely, the orbital effects leading to H_{c2} are almost always present, even in strongly quasi-2D materials in magnetic fields parallel to the 2D planes. Perhaps, an ideal realization of this state would be surface superconductivity or superconductivity in thin films in fields parallel to the surface. We note, however, that unlike the LOFF state, which is difficult to observe, since it quickly disappears in the presence of impurities or orbital effects, the homogeneous partially gapless state is more robust, and will appear in many multiband strongly quasi-2D *s*-wave superconductors in the mixed state as well, provided that the upper critical field is close enough to the Clogston limit. The details of such first-order transition in the mixed state will be similar to the physics considered above. Measurements of the specific heat in applied field are the most direct way to observe the low-field first-order phase transition in *s*-wave multiband superconductors, such as 2H-$NbSe_2$.[21] Paramagnetic pair breaking also appears in the presence of ferromagnetic ordering as a result of exchange coupling between localized moments and delocalized carriers, such as in the original model of.[41] Thus, an observation,[83] by scanning tunneling spectroscopy, of large gapless regions of Fermi surface in superconducting $ErNi_2B_2C$, a borocarbide multiband material where weak ferromagnetism coexists with superconductivity, is quite interesting and possibly related to the effects of pair breaking on the very small gap on one of the Fermi surfaces discussed in this paper or in Ref. 27.

ACKNOWLEDGMENTS

The author is very grateful to L.P. Gor'kov for many discussions, and to A.V. Sologubenko and H. Suderow for sharing new experimental results. This work was supported by TAML at the University of Tennessee and by NHFML through the NSF under Cooperative Agreement No. DMR-008473 and the State of Florida.

[1] H. Suhl, B. T. Matthias, and L. R. Walker, Phys. Rev. Lett. **3**, 552 (1959).
[2] V. A. Moskalenko, Fiz. Met. Metalloved. **8**, 503 (1959); Phys. Met. Metallogr. **8**, 25 (1959).
[3] B. T. Geilikman, R. O. Zaitsev, and V. Z. Kresin, Fiz. Tverd. Tela (St. Petersburg) **9**, 821 (1967); Sov. Phys. Solid State **9**, 642 (1967).
[4] V. Z. Kresin, J. Low Temp. Phys. **11**, 519 (1973).
[5] M. L. Cohen, in *Superconductivity*, edited by R. D. Parks (Dekker, New York, 1969), Vol. 1, p. 615.
[6] J. Nagamatsu, N. Nakagawa, T. Muranaka, Y. Zenitani, and J. Akimitsu, Nature (London) **410**, 63 (2001).
[7] F. Giubileo, D. Roditchev, W. Sacks, R. Lamy, D. X. Thanh, J. Klein, S. Miraglia, D. Fruchart, J. Marcus, and P. Monod, Phys. Rev. Lett. **87**, 177008 (2001).
[8] M. Iavarone, G. Karapetrov, A. E. Koshelev, W. K. Kwok, G. W. Crabtree, D. G. Hinks, W. N. Kang, E.-M. Choi, H. J. Kim, H. J. Kim, and S. I. Lee, Phys. Rev. Lett. **89**, 187002 (2002).
[9] P. Szabo, P. Samuely, J. Kacmarcik, T. Klein, J. Marcus, D. Fruchart, S. Miraglia, C. Marcenat, and A. G. M. Jansen, Phys. Rev. Lett. **87**, 137005 (2001).
[10] H. Schmidt, J. F. Zasadzinski, K. E. Gray, and D. G. Hinks, Phys. Rev. Lett. **88**, 127002 (2002).
[11] Y. Wang, T. Plackowski, and A. Junod, Physica C **355**, 179 (2001).
[12] F. Bouquet, R. A. Fisher, N. E. Phillips, D. G. Hinks, and J. D. Jorgensen, Phys. Rev. Lett. **87**, 047001 (2001).
[13] H. D. Yang, J.-Y. Lin, H. H. Li, F. H. Hsu, C. J. Liu, S.-C. Li, R.-C. Yu, and C.-Q. Jin, Phys. Rev. Lett. **87**, 167003 (2001).
[14] F. Bouquet, Y. Wang, R. A. Fisher, D. G. Hinks, J. D. Jorgensen, A. Junod, and N. E. Phillips, Europhys. Lett. **56**, 856 (2001).
[15] Y. Kamihara, T. Watanabe, M. Hirano, and H. Hosono, J. Am. Chem. Soc. **130**, 3296 (2008).
[16] I. A. Nekrasov, Z. V. Pchelkina, and M. V. Sadovskii, JETP Lett. **87**, 560 (2008).
[17] D. J. Singh and M.-H. Du, Phys. Rev. Lett. **100**, 237003 (2008).
[18] I. I. Mazin, D. J. Singh, M. D. Johannes, and M. H. Du, Phys. Rev. Lett. **101**, 057003 (2008).
[19] V. Barzykin and L. P. Gor'kov, JETP Lett. **88**, 131 (2008).
[20] M. D. Johannes, I. I. Mazin, and C. A. Howells, Phys. Rev. B **73**, 205102 (2006).
[21] T. Yokoya, T. Kiss, A. Chainani, S. Shin, M. Nohara, and H. Takagi, Science **294**, 2518 (2001).
[22] J. D. Fletcher, A. Carrington, P. Diener, P. Rodiere, J. P. Brison, R. Prozorov, T. Olheiser, and R. W. Giannetta, Phys. Rev. Lett. **98**, 057003 (2007).
[23] M. E. Zhitomirsky and V.-H. Dao, Phys. Rev. B **69**, 054508 (2004).
[24] A. E. Koshelev and A. A. Golubov, Phys. Rev. Lett. **92**, 107008 (2004).

[25] A. A. Abrikosov and L. P. Gor'kov, Zh. Eksp. Teor. Fiz. **39**, 1781 (1960) [Sov. Phys. JETP **12**, 1243 (1960)].
[26] M. A. Tanatar, J. Paglione, S. Nakatsuji, D. G. Hawthorn, E. Boaknin, R. W. Hill, F. Ronning, M. Sutherland, L. Taillefer, C. Petrovic, P. C. Canfield, and Z. Fisk, Phys. Rev. Lett. **95**, 067002 (2005).
[27] V. Barzykin and L. P. Gor'kov, Phys. Rev. B **76**, 014509 (2007).
[28] For a review, see V. P. Mineev, Int. J. Mod. Phys. B **18**, 2963 (2004).
[29] P. A. Frigeri, D. F. Agterberg, A. Koga, and M. Sigrist, Phys. Rev. Lett. **92**, 097001 (2004).
[30] E. Bauer, G. Hilscher, H. Michor, Ch. Paul, E. W. Scheidt, A. Gribanov, Yu. Seropegin, H. Noel, M. Sigrist, and P. Rogl, Phys. Rev. Lett. **92**, 027003 (2004).
[31] S. S. Saxena, P. Agarval, K. Ahilan, F. M. Grosche, R. K. W. Hasselwimmer, M. J. Steiner, E. Pugh, I. R. Walker, S. R. Julian, P. Monthoux, G. G. Lonzarich, A. Huxley, I. Sheikin, D. Braithwaite, and J. Flouquet, Nature (London) **406**, 587 (2000).
[32] A. Huxley, E. Ressouche, B. Grenier, D. Aoki, J. Floquet, and C. Pfleiderer, J. Phys.: Condens. Matter **15**, S1945 (2003).
[33] C. Pfleiderer, M. Uhlarz, S. Heiden, R. Vollmer, H. v. Lohneysen, N. R. Bernhoeft, and G. G. Lonzarich, Nature (London) **412**, 58 (2001).
[34] D. Aoki, A. Huxley, E. Ressouche, D. Braithwaite, J. Flouquet, J.-P. Brison, E. Lhotel, and C. Paulsen, Nature (London) **413**, 613 (2001).
[35] L. P. Gor'kov and E. I. Rashba, Phys. Rev. Lett. **87**, 037004 (2001).
[36] V. Barzykin and L. P. Gor'kov, Phys. Rev. Lett. **89**, 227002 (2002).
[37] E. I. Rashba, Sov. Phys. Solid State **2**, 1109 (1960).
[38] Yu. A. Bychkov and E. I. Rashba, Pis'ma Zh. Eksp. Teor. Fiz. **39**, 66 (1984) [JETP Lett. **39**, 78 (1984)].
[39] A. M. Clogston, Phys. Rev. Lett. **9**, 266 (1962).
[40] B. S. Chandrasekhar, Appl. Phys. Lett. **1**, 7 (1962).
[41] A. I. Larkin and Yu. N. Ovchinnikov, Zh. Eksp. Teor. Fiz. **47**, 1136 (1964) [Sov. Phys. JETP **20**, 762 (1965)].
[42] P. Fulde and R. A. Ferrell, Phys. Rev. **135**, A550 (1964).
[43] G. Sarma, J. Phys. Chem. Solids **24**, 1029 (1963).
[44] S. Takada and T. Izuyama, Prog. Theor. Phys. **41**, 635 (1969).
[45] J. Hessert, M. Huth, M. Jourdan, H. Adrian, C. T. Rieck, and K. Scharnberg, Physica B **230-232**, 373 (1997).
[46] I. A. Garifullin, J. Magn. Magn. Mater. **240**, 571 (2002).
[47] M. Aprili, T. Kontos, M.-L. Della Rocca, J. Lesueur, W. Guichard, P. Gandit, A. Bauer, and C. Strunk, C. R. Phys. **7**, 116 (2006).
[48] J. Singleton, Rep. Prog. Phys. **63**, 1111 (2000).
[49] C. Capan, A. Bianchi, R. Movshovich, A. D. Christianson, A. Malinowski, M. F. Hundley, A. Lacerda, P. G. Pagliuso, and J. L. Sarrao, Phys. Rev. B **70**, 134513 (2004).
[50] Kun Yang, in *Pairing in Fermionic Systems: Basic Concepts and Modern Applications*, edited by M. Alford, J. Clark, and A. Sedrakian (World Scientific, Singapore, 2006), p. 253.
[51] T. Mizushima, K. Machida, and M. Ichioka, Phys. Rev. Lett. **95**, 117003 (2005).
[52] K. Kakuyanagi, M. Saitoh, K. Kumagai, S. Takashima, M. Nohara, H. Takagi, and Y. Matsuda, Phys. Rev. Lett. **94**, 047602 (2005).
[53] V. F. Mitrović, M. Horvatić, C. Berthier, G. Knebel, G. Lapertot, and J. Flouquet, Phys. Rev. Lett. **97**, 117002 (2006).
[54] R. Casalbuoni and G. Nardulli, Rev. Mod. Phys. **76**, 263 (2004).
[55] W. V. Liu and F. Wilczek, Phys. Rev. Lett. **90**, 047002 (2003).
[56] M. Alford, K. Rajagopal, and F. Wilczek, Nucl. Phys. B **537**, 443 (1999).
[57] E. Gubankova, W. V. Liu, and F. Wilczek, Phys. Rev. Lett. **91**, 032001 (2003).
[58] E. Gubankova, E. G. Mishchenko, and F. Wilczek, Phys. Rev. Lett. **94**, 110402 (2005).
[59] W. Baltensperger, Helv. Phys. Acta **32**, 197 (1959).
[60] L. P. Gor'kov and A. I. Rusinov, Zh. Eksp. Teor. Fiz. **46**, 1363 (1964) [Sov. Phys. JETP **19**, 922 (1964)].
[61] L. V. Butov, A. S. Gossard, and D. S. Chemla, Nature (London) **418**, 751 (2002).
[62] L. V. Butov, L. S. Levitov, A. V. Mintsev, B. D. Simons, A. C. Gossard, and D. S. Chemla, Phys. Rev. Lett. **92**, 117404 (2004).
[63] M. E. Zhitomirsky, T. M. Rice, and V. I. Anisimov, Nature (London) **402**, 251 (1999).
[64] B. A. Volkov, Yu. V. Kopaev, and A. I. Rusinov, Zh. Eksp. Teor. Fiz. **68**, 1899 (1975) [Sov. Phys. JETP **41**, 952 (1976)].
[65] L. P. Gor'kov and T. T. Mnatsakanov, Zh. Eksp. Teor. Fiz. **63**, 684 (1972) [Sov. Phys. JETP **36**, 361 (1973)].
[66] V. Barzykin and L. P. Gor'kov, Phys. Rev. Lett. **84**, 2207 (2000).
[67] L. Balents and C. M. Varma, Phys. Rev. Lett. **84**, 1264 (2000).
[68] N. I. Karchev, K. B. Blagoev, K. S. Bedell, and P. B. Littlewood, Phys. Rev. Lett. **86**, 846 (2001).
[69] Y. N. Joglekar and A. H. MacDonald, Phys. Rev. Lett. **92**, 199705 (2004).
[70] K. B. Blagoev, K. S. Bedell, and P. B. Littlewood, Phys. Rev. Lett. **92**, 199706 (2004).
[71] V. Barzykin and L. P. Gor'kov, Phys. Rev. Lett. **98**, 087004 (2007).
[72] D. F. Agterberg, V. Barzykin, and L. P. Gor'kov, Phys. Rev. B **60**, 14868 (1999); Europhys. Lett. **48**, 449 (1999).
[73] A. A. Abrikosov, L. P. Gor'kov, and I. E. Dzyaloshinskii, *Methods of Quantum Field Theory in Statistical Physics* (Dover, New York, 1963).
[74] Ye Sun and K. Maki, Phys. Rev. B **51**, 6059 (1995).
[75] V. L. Pokrovskii, Zh. Eksp. Teor. Fiz. **40**, 641 (1961) [Sov. Phys. JETP **13**, 447 (1961)].
[76] G. E. Volovik and L. P. Gor'kov, Pis'ma Zh. Eksp. Teor. Fiz. **39**, 550 (1984) [JETP Lett. **39**, 674 (1984)]; Zh. Eksp. Teor. Fiz. **88**, 1412 (1985) [Sov. Phys. JETP **61**, 843 (1985)].
[77] L. P. Gor'kov, Sov. Sci. Rev., Sect. A **9**, 1 (1987).
[78] V. Kuznetsova and V. Barzykin, Europhys. Lett. **72**, 437 (2005).
[79] V. Barzykin and L. P. Gor'kov (unpublished).
[80] H. Burkhardt and D. Rainer, Ann. Phys. **3**, 181 (1994).
[81] A. V. Sologubenko, I. L. Landau, H. R. Ott, A. Bilusic, A. Smontara, and H. Berger, Phys. Rev. Lett. **91**, 197005 (2003).
[82] L. N. Bulaevskii, A. A. Guseinov, and A. I. Rusinov, Zh. Eksp. Teor. Fiz. **71**, 2356 (1976) [Sov. Phys. JETP **44**, 1243 (1976)].
[83] M. Crespo, H. Suderow, S. Vieira, S. Bud'ko, and P. C. Canfield, Phys. Rev. Lett. **96**, 027003 (2006).